



1 **Significant spatial and temporal variation of the concentrations**
2 **and chemical composition of ultrafine particulate matter over**
3 **Europe**

4
5
6 Konstantinos Mataras^{1*}, Evangelia Siouti^{2*}, David Patoulias² and Spyros N. Pandis^{1,2}

7 ¹Department of Chemical Engineering, University of Patras, Patras, Greece

8 ²Institute of Chemical Engineering Sciences (ICE-HT), Foundation for Research and Technology Hellas (FORTH), Patras,
9 Greece

10 *These two authors contributed equally to this work.

11 *Correspondence to:* Spyros N. Pandis (spyros@chemeng.upatras.gr)

12 **Abstract.** Ultrafine particles have attracted interest as perhaps the most dangerous fraction of atmospheric PM. This study
13 focuses on the characterization of ultrafine particulate matter (PM_{0.1}) mass concentrations and their chemical composition
14 during a summer and winter period in Europe.

15 Predicted levels of PM_{0.1} varied substantially, both in space and in time. The average predicted PM_{0.1} mass
16 concentration was 0.6 µg m⁻³ in the summer, higher than the 0.3 µg m⁻³ predicted in the winter period. PM_{0.1} chemical
17 composition exhibited significant seasonality. In summer, PM_{0.1} was mostly comprised of secondary inorganic matter
18 (38% sulfate and 13% ammonium) and organics (9% primary and 32% secondary). During the winter, the fraction of
19 secondary inorganic matter increased, with sulfate contributing 47% and ammonium 19%, on average. Primary organic
20 matter contribution also increased from 9% in summer to 23% in winter, while secondary organic matter decreased
21 significantly to 6% on average during winter.

22 During summertime, the model performance at 12 sites for daily average ultrafine particle volume (PV_{0.1})
23 concentrations was considered good, with normalized mean error (NME) equal to 46% and normalized mean bias (NMB)
24 equal to 15%. For the winter period, the corresponding values for daily average levels were -27% for NMB and 64% for
25 NME, indicating an average model performance.

26 Correlations between PM_{0.1} and the currently regulated PM_{2.5} were generally low. Better correlations were
27 observed in cases where the primary component of PM_{0.1} was significant. This suggests that there are significant
28 differences between the dominant sources and processes of PM_{0.1} and PM_{2.5}.

29

30 **1. Introduction**

31 UFPs dominate atmospheric particle number distribution (Seinfeld and Pandis, 2006). High concentrations of both UFP
32 number and mass are found in urban areas and are a result of human activity, directly emitting particulates or producing
33 them by gas-to-particle conversion processes. Atmospheric particle exposure is one of the most significant risk factors
34 affecting human health (HEI, 2013; EPA, 2019). Ultrafine particles have attracted interest because they may be the most
35 dangerous fraction of atmospheric particulate matter. They can reach the lung alveoli, pass into the bloodstream and from
36 there they can move to many different organs (Schraufnagel, 2020; Sioutas et al., 2005). Their increased specific surface
37 area with decreasing size also enhances their chemical and physical interactions, both with gaseous species outside the
38 body and also with tissues inside the body (Kwon et al., 2020). Some epidemiological studies have noted a positive



39 correlation between UFPs exposure and brain tumor incidence (Weichenthal et al., 2020). However, there are still
40 questions about the links between ultrafine particle exposure and damage to human health (EPA, 2019).

41 Past studies of ultrafine particles have focused on their number concentrations (Baranizadeh et al., 2016;
42 Merikanto et al., 2009; Patoulias et al., 2015, 2018; Wang and Penner, 2009; Yu and Luo, 2009). The comparatively scarce
43 modelling attempts aimed at ultrafine particle mass have mostly been conducted in California and the US (Hu et al.,
44 2014a, b, 2017; Venecek et al., 2019; Yu et al., 2019).

45 In the study by Hu et al. (2014a, b) for the 7-year (2000-2006) period, daily predictions of primary $PM_{0.1}$ from
46 the UCD-P model were evaluated for California. They found good agreement of model predictions with observed $PM_{0.1}$
47 mass and elemental carbon (Kuwayama et al., 2013), with a Pearson correlation coefficient ($R > 0.92$) during these periods.
48 They reported model difficulties in reproducing observed values of $PM_{0.1} > 4 \mu g m^{-3}$ or $< 1 \mu g m^{-3}$. In a subsequent study
49 of $PM_{0.1}$, Hu et al. (2017) utilized again the UCD/CIT model. The authors reported that primary organic matter was the
50 major component (50-90%) of $PM_{0.1}$ OA in California, with 9-year average concentrations above $2 \mu g m^{-3}$ in major urban
51 areas. They predicted that secondary organics contribute less than 10% to $PM_{0.1}$ OA in these areas, with that contribution
52 increasing to up to 50% in rural areas, with low organic matter content. $PM_{0.1}$ secondary organic aerosol (SOA)
53 concentrations were predicted to be mostly biogenic (64% of SOA for the domain) and between $0.02-0.05 \mu g m^{-3}$ in the
54 winter and $0.1-0.3 \mu g m^{-3}$ in the summer. Underprediction of secondary organic aerosol concentrations was proposed as
55 an explanation of the $PM_{0.1}$ organic mass underprediction. Yu et al. (2019) along with Venecek et al. (2019) considered
56 nucleation along with the rest of the major aerosol processes in a $PM_{0.1}$ study. Venecek et al. (2019) investigated $PM_{0.1}$
57 concentration and sources during summertime pollution events in several metropolitan areas of the US. Predicted daily
58 average $PM_{0.1}$ levels were generally above $2 \mu g m^{-3}$, reaching $5 \mu g m^{-3}$ in areas influenced by wildfire events. The $PM_{0.1}$
59 spatial gradients were much sharper than those of $PM_{2.5}$ due to the dominance of the primary $PM_{0.1}$. The dominant source
60 of $PM_{0.1}$ was found to be natural gas combustion across all major cities in the US. Yu et al. (2019) studied UFP number
61 as well as mass concentrations and sources in California. Xue et al. (2019) reported that meat cooking was a major source
62 of $PM_{0.1}$ organic carbon across all California cities (13–29%), while nucleation contributed negligibly to UFP mass on an
63 annual scale.

64 Experimental studies investigating ultrafine particles have focused on particle number concentrations and their
65 spatial and temporal differences. The first detailed measurements of UFP mass have been performed in California
66 (Bernardoni et al., 2017; Kuwayama et al., 2013; Xue et al., 2018, 2019, 2020a, b; Xue and Kleeman, 2022). In these
67 studies, researchers collected one sample every day or used even longer averaging intervals because of the low UFP mass
68 concentrations. Hughes et al. (1998) reported daily average mass concentrations varying from 0.8 to $1.6 \mu g m^{-3}$ in
69 Pasadena, CA. A novel method to measure UFP mass continuously has been recently developed and tested by
70 Argyropoulou et al. (2023, 2024), but has not been applied in field studies yet.

71 Major sources of $PM_{0.1}$ in the US include vehicular emissions (Bernardoni et al., 2017; Hu et al., 2014a), biomass
72 (wood burning and meat cooking) burning (Kleeman et al., 2009) but also natural gas combustion (Xue et al., 2018) and
73 aviation in areas close to airports (Venecek et al., 2019). Relatively little is known in areas outside the US about ultrafine
74 particle properties other than their number concentrations and size distribution (del Águila et al., 2018; Putaud et al.,
75 2010).

76 The few studies, however, using $PM_{0.1}$ as the exposure metric have shown positive correlations of ultrafine
77 particle organic and trace metal components with negative health effects (Laurent et al., 2016; Ostro et al., 2015). For



78 UFP mass, field studies as well as modelling studies have been largely restricted to California or parts of Asia, which are
79 dominated by primary sources (Phairuang et al., 2022; Xue et al., 2019, 2020b; Zhu et al., 2002). As such, large
80 uncertainties about their health effects still remain (Delfino et al., 2005; EPA, 2019; Ohlwein et al., 2019).

81 In this work, $PM_{0.1}$ mass concentrations as well as their chemical composition were studied during a typical
82 summer (5 June - 8 July 2012) and winter period (1-30 January 2009) for several urban and rural sites in Europe using
83 the PMCAMx-UF chemical transport model. Due to the difficulty of measuring $PM_{0.1}$ mass, $PV_{0.1}$ is used in this study to
84 evaluate the model predictions on an hourly and daily scale.

85

86 2. Model description

87 PMCAMx-UF is an Eulerian regional three-dimensional chemical transport model (Jung et al., 2010) that is an extension
88 of the PMCAMx model (Gaydos et al., 2007). The extended Dynamic Model for Aerosol Nucleation (DMANx) module
89 is used in PMCAMx-UF for the better description of ambient ultrafine particulate matter processes (Patoulias et al., 2015).
90 PMCAMx-UF solves the mass conservation equation for each pollutant in the gas, aqueous and particulate phases
91 focusing especially on the aerosol number and mass size distributions and the ultrafine particles.

92 Processes simulated by PMCAMx-UF include transport of pollutants via advection and eddy diffusion, their
93 chemical transformation in the gas, aerosol and aqueous (cloud) phases, their removal from the atmosphere through dry
94 (without water involvement) and wet (with water involvement) processes, their introduction into the atmosphere by direct
95 emission, whether from natural planetary processes or by human activity, and lastly specific physical processes for the
96 particle phase, namely coagulation, condensation/evaporation and nucleation. PMCAMx-UF simulates the temporal
97 variation of the complete aerosol number size distribution, beginning from particles as small as 0.8 nm and up to 10 μm .
98 At the same time, the mass concentration of 18 major aerosol components is simulated, including inorganics (ammonium,
99 sulfate, metals, nitrate, sodium, chloride), primary and secondary organic aerosol, elemental carbon and aerosol phase
100 water. The secondary organic aerosol species are split into 4 volatility bins for the anthropogenic and another 4 for those
101 of biogenic origin. An extremely low volatility secondary organic aerosol component was added by Patoulias and Pandis
102 (2022) to simulate the extremely low volatility secondary organic compounds.

103 Gas phase chemistry in PMCAMx-UF is described by the extended Statewide Air Pollution Research Center
104 (SAPRC) mechanism (ENVIRON, 2003; Patoulias and Pandis, 2022), which involves 219 thermochemical and
105 photochemical reactions, 64 gaseous compounds, of which 11 reactivity lumped organic compounds (5 alkanes, 2 olefins,
106 2 aromatics, a mono- and a sesqui-terpene) and 18 free radicals. PMCAMx-UF utilizes the variable sizes resolution
107 (VRSM) aqueous phase chemical module (Fahey and Pandis, 2001). The algorithm for horizontal advection is based on
108 the piecewise parabolic method of Colella and Woodward (1984) and its implementation by Odman and Ingram (1996).
109 Dry deposition is described by a first order kinetic removal rate. For gaseous pollutants, the dry deposition velocity is
110 calculated from the series resistance to impaction model of Wesely (1989). For aerosol species, the gravitational settling
111 velocity is in addition factored in. Its calculation follows the implementation of Slinn and Slinn (1980). Additional
112 information about PMCAMx-UF can be found in Patoulias et al. (2018).

113

114 3. Model application

115 PMCAMx-UF was applied to a modelling domain spanning the European continental area, covering a 5400x5832 km^2
116 area, using a rotated polar stereographic domain projection. This region is divided into 36x36 km^2 cells resulting in 24300



117 cells in each vertical level. In the vertical axis there are 14 levels, extending to approximately 7.2 km. The ground level,
118 which is the main focus of this study, has a 60 m top boundary height.

119 The two periods examined correspond to 5 June to 8 July 2012 and 1 to 30 January 2009, during the PEGASOS
120 and EUCAARI campaigns respectively. Inputs for this version of PMCAMx-UF and specifically for the studied periods
121 have been described by Patoulias and Pandis (2022).

122 Meteorological input data for both periods were generated by the Weather Research and Forecasting (WRFv2)
123 model (Skamarock et al., 2005). This model utilizes geospatial time-varying meteorology data as inputs that are a product
124 of the Global Forecast System (GFSv15) of the National Oceanic and Atmospheric Administration (NOAA). WRF model
125 grids correspond to those of the chemical transport model.

126 Anthropogenic particulate matter emissions have hourly space resolution and are based on the pan-European
127 anthropogenic particle number emissions inventory and the carbonaceous aerosol inventory, both developed during the
128 European Integrated project on Aerosol, Cloud, Climate, and Air Quality Interactions (EUCAARI) (Kulmala et al., 2011).
129 These datasets include various anthropogenic sources such as ground transportation, shipping, industrial processes,
130 domestic activities, etc. Anthropogenic gas-phase emissions are based on the Global and regional Earth-system
131 Monitoring using satellite and in situ data (GEMS) inventory. Continental natural ecosystem emissions were derived
132 using the Model of Emissions of Gases and Aerosol from Nature (MEGANv2.1) (Guenther et al., 2006). MEGAN requires
133 the meteorological inputs described above, as well as surface area type indicators. Natural marine emissions are based on
134 the model of O'Dowd et al. (2008). Wildfire emissions included in our simulation were taken from the Sofiev et al. (2008a,
135 b) emission inventory. Intermediate volatility organic compound emissions were estimated based on the primary organic
136 aerosol emission rates, with proportionality factors depending on estimated volatility (Patoulias and Pandis, 2022).

137 Initial and boundary conditions used in this application were constant and low to minimize their influence on
138 model predictions. The first two days of the summer and winter simulation periods are not included in the analysis. This
139 is a time interval which has been shown to be adequate to exclude most of the influence of initial conditions in previous
140 PMCAMx-UF applications (Patoulias et al., 2018; Patoulias and Pandis, 2022).

141

142 **3.1 Measurements**

143 Ultrafine particle mass is difficult to measure, primarily due to its low concentration. In order to evaluate hourly model
144 predictions of ultrafine particulate matter concentrations, we use here surface level measurements of particle number size
145 distributions, available through the EBAS database (<https://ebas-data.nilu.no>), during the Pan-European-Gas-AeroSol-
146 climate interaction Study (PEGASOS) and the European Integrated project on Aerosol, Cloud, Climate, and Air Quality
147 Interactions (EUCAARI) (Kulmala et al., 2011) intensive measurement campaigns. The locations of the 12 measurement
148 sites are shown in Figure 1. These include Mace Head (Ireland), Varrio, Hyytiala (Finland), Aspvreten, Vavihill (Sweden),
149 Helsinki (Finland), Waldhof, Melpitz, Dresden, Hohenpeissenberg (Germany), Kosetice (Czech Republic) and Finokalia
150 (Greece). Particle number distribution measurements in each site were made through mobility particle sizers, either
151 scanning (SMPS) or differential (DMPS). The ultrafine particle volume concentrations, $PV_{0.1}$, was then calculated by
152 integrating these distributions up to 100 nm assuming spherical particles. The $PM_{0.1}$ concentration can be calculated by
153 multiplying with an average UFP density. However, to avoid complications $PV_{0.1}$ will be used directly for the model
154 evaluation.



155 The $PM_{0.1}$ predicted by PMCAMx-UF was converted to $PV_{0.1}$ by estimating the average ultrafine particle density,
156 ρ_{UFP} , based on the predicted particle composition at each point at time:

$$159 \quad PV_{0.1} = \frac{PM_{0.1}}{\rho_{UFP}} \quad (1)$$

$$160 \quad \rho_{UFP} = \frac{\sum_{i=1}^N \rho_i PM_{0.1,i}}{PM_{0.1}} \quad (2)$$

161 where N is the total number of components, ρ_i is the density of component i , $PM_{0.1,i}$ is the $PM_{0.1}$ mass concentration of
162 component i , and the total $PM_{0.1}$ the total mass concentration.

163

164 4. Results

165 4.1 Average spatial variation of $PM_{0.1}$

166 The average $PM_{0.1}$ predictions at the ground level during the summertime simulated period are shown in Figure 2. There
167 was considerable spatial variability of $PM_{0.1}$ levels throughout Europe. The average predicted $PM_{0.1}$ in the modeling
168 domain was $0.4 \mu\text{g m}^{-3}$. The mean value was heavily influenced by the fact that a significant part of the domain is over
169 the Atlantic Ocean and Northern Africa, regions with much lower concentrations of $PM_{0.1}$. Averaging without those parts
170 of the domain increased $PM_{0.1}$ to $0.6 \mu\text{g m}^{-3}$.

171 $PM_{0.1}$ was predicted to have higher values, up to $1.2 \mu\text{g m}^{-3}$, in parts of southern and eastern Europe. High levels
172 were also predicted for major urban areas like Paris, as well as areas with high ship traffic like the North Sea or the
173 western Mediterranean. $PM_{0.1}$ was predicted to be, on average, 51% secondary inorganic matter (38% sulfate and 13%
174 ammonium), 41% organic matter (9% primary and 32% secondary), with smaller contributions from elemental carbon
175 (5%), metal oxides (2%) and trace contributions (<1%) of nitrate, sodium and chloride. Sulfate levels were higher in the
176 North Sea, the Mediterranean, parts of the Middle East and the Strait of Gibraltar, as well as the lower Bay of Biscay.
177 Ammonium spatial patterns mirror those of sulfate. SOA was a major $PM_{0.1}$ contributor in most of eastern and central
178 Europe. POA and elemental carbon contributed relatively little mass on the domain scale, with sharp spatial gradients in
179 regions of increased human activity.

180 The average predicted $PM_{0.1}$ concentration and composition for the winter period are shown in Figure 3. $PM_{0.1}$
181 levels were on average lower across the domain, with a mean domain value of $0.18 \mu\text{g m}^{-3}$. The average level over Europe
182 was $0.3 \mu\text{g m}^{-3}$.

183 Wintertime $PM_{0.1}$ was predicted to consist of an average of 66% secondary inorganic material (47% sulphate and
184 19% ammonium), 23% primary matter (9% elemental carbon, 9% organic matter and 5% metals), with small amounts of
185 nitrate, sodium and chloride (<5%). SOA contributed 6% to the mean predicted $PM_{0.1}$, with higher contribution in
186 northwestern Russia, northern Italy and southern Spain and Portugal. The highest SOA average concentration was $0.1 \mu\text{g}$
187 m^{-3} in northwestern Russia. $PM_{0.1}$ in central and western Europe, as well as in key urban areas of the Iberian Peninsula
188 and northern Italy, was mainly composed of primary (emitted) matter. Primary matter concentration was as high as 0.9
189 $\mu\text{g m}^{-3}$ in urban areas. Sulfate, and the associated ammonium, were the major contributors to $PM_{0.1}$ in eastern Europe
190 according to PMCAMx-UF, however with reduced concentration relative to the summer. The $PM_{0.1}$ levels in northwestern
191 and central Europe were lower by around $0.2 \mu\text{g m}^{-3}$ compared to the summer. In southern Italy, the concentrations were



192 reduced from more than $1 \mu\text{g m}^{-3}$ to less than $0.4 \mu\text{g m}^{-3}$. On the other hand, in many urban areas (e.g. Paris) the $\text{PM}_{0.1}$
193 levels were similar or even higher during the winter.

194

195 **4.2 Predicted $\text{PM}_{0.1}$ chemical composition in urban areas**

196 The average predicted chemical composition of $\text{PM}_{0.1}$ for selected sites is depicted in Figure 4 for the summer and winter
197 period. Sulfate was a major $\text{PM}_{0.1}$ component during the summer, with its fractional mass contribution varying from 17%
198 to 51% depending on location. Ammonium (7-16%), primary organics (4-16%), elemental carbon (2-29%) and metals (1-
199 5%) were the remaining major contributors. SOA contributed from 2 to 10%. The mass percentage of sodium, chloride
200 and nitrate was in most sites less than 1%. The predicted $\text{PM}_{0.1}$ summertime concentration was mostly (52% to 91%)
201 secondary (organic or inorganic). A significant fraction of the SOA (40-73%) was predicted to be anthropogenic in all
202 sites (Table S3).

203 In the urban area of Athens, the major component of $\text{PM}_{0.1}$ was sulfate (35%), followed by SOA (23%), primary
204 organic aerosol (POA) (16%) and ammonium (13%). In Paris, elemental carbon had the highest contribution (30%) to
205 $\text{PM}_{0.1}$. Sulfate contributed 20% and SOA 20%. At the rural site of Finokalia, $\text{PM}_{0.1}$ consisted of 51% sulfate, 27% SOA
206 and 20% ammonium, with smaller contributions of elemental carbon (2%) and primary organic aerosol (4%).

207 During the winter period, primary material contributed from 22% to 61% to $\text{PM}_{0.1}$ depending on location (Fig.
208 4). Primary organic aerosol ranged from 10% to 23%. Elemental carbon was predicted to contribute 8% to 31%, while
209 metals from 4% to 10% across all sites. Ammonium and sulfate remained a significant fraction of $\text{PM}_{0.1}$ (33% to 69%),
210 especially in the urban areas in eastern Europe. The sulfate fraction ranged from 24% to 49%, with ammonium
211 contributing from 9% to 20%. The contribution of SOA was limited, up to 9% at the sites examined. The remaining $\text{PM}_{0.1}$
212 components, namely nitrate, chloride and sodium, were predicted to contribute up to 1% in almost all the examined sites.

213 In Athens, wintertime $\text{PM}_{0.1}$ consisted of sulfate (37%), POA (23%), elemental carbon (15%) and ammonium
214 (13%). The remaining were metals (7%) and SOA (5%). In Paris, elemental carbon was the major $\text{PM}_{0.1}$ component with
215 a contribution of 30%. Sulfate contributed 25%, while POA 20%. Lower contributions were predicted for ammonium
216 (10%), metals (10%) and SOA (5%). At the rural site of Finokalia, $\text{PM}_{0.1}$ mainly consisted of sulfate (49%) and ammonium
217 (16%), with smaller contributions of primary organic aerosol (10%), elemental carbon (8%), chloride and sodium.

218

219 **4.3 PMCAMx-UF evaluation**

220 *4.3.1 Summer*

221 During the summer period, PMCAMx-UF predictions showed on average little bias with a NMB equal to 15% for hourly
222 average concentrations (Table 1). The NME, on an hourly level, was on average 62%, a level similar to that of $\text{PM}_{2.5}$
223 predictions of CTMs in Europe. The model performance in this first application was clearly quite encouraging. NMB and
224 NME hourly metrics in the various stations ranged from -29% to +109% and from +44% to +125%, respectively. The
225 model's performance improved, as expected, for daily average concentrations (Table S1). The NME was reduced to 46%.
226 The NMB remained at the low level of 15%. This performance was considered very good with the evaluation criteria of
227 fine PM (Morris et al., 2005).

228 During the summer, for most locations, model predictions as well as measured values exhibited significant
229 variability (Fig. 5). In most sites, the mean was larger than the median due to short-term elevated concentrations.
230 PMCAMx-UF on average did a reasonable job reproducing the observations, with overpredictions and underpredictions



231 of $PV_{0.1}$, depending on the location. Average concentrations for the full period were captured within $0.1 \mu\text{m}^3 \text{cm}^{-3}$ for 7
232 out of 12 of the examined sites, with all the predicted averages being within $0.25 \mu\text{m}^3 \text{cm}^{-3}$ of measurements. Focusing
233 on the urban sites, in Dresden, mean ultrafine particle volume concentration was underpredicted by $0.17 \mu\text{m}^3 \text{cm}^{-3}$. For
234 Helsinki, the mean predicted $PV_{0.1}$ was quite consistent with the measurements. The distributions of $PV_{0.1}$ were also in
235 good agreement. In Kosetice, the model overpredicted by $0.13 \mu\text{m}^3 \text{cm}^{-3}$. Also, the predicted concentrations were in
236 general higher than the measurements. Mean predicted $PV_{0.1}$ for all the sites examined was $0.34 \mu\text{m}^3 \text{cm}^{-3}$ and the
237 corresponding measured value was $0.29 \mu\text{m}^3 \text{cm}^{-3}$. PMCAMx-UF overpredicted by 0.13 to $0.25 \mu\text{m}^3 \text{cm}^{-3}$ in the Vavihill,
238 Aspvreten, Waldhof and Kosetice sites, all rural background areas in central and northern Europe.

239 In Dresden, the model predicted a weaker diurnal variation to that observed, but its main weakness was its
240 underprediction of the baseline by around $0.2 \mu\text{m}^3 \text{cm}^{-3}$ (Fig. 6). A noticeable measured peak at 8:00 LST probably
241 indicates traffic emissions which were not captured in the model, either through omission or due to grid resolution. The
242 model tended overall to capture the hourly variations (Fig. S1), though it missed some high concentration periods on June
243 the 8, 10, 16 and 24.

244 For Helsinki, the average measured diurnal pattern was relatively flat (Fig. 6). Measured values were reproduced
245 well by PMCAMx-UF, with differences of around $0.05 \mu\text{m}^3 \text{cm}^{-3}$ throughout most of the average day. The detailed time
246 series was also well reproduced (Fig. S1).

247 In Kosetice, for the first half of the day, predictions were far larger than the corresponding measurements, starting
248 the night at $+0.1 \mu\text{m}^3 \text{cm}^{-3}$ and peaking at 05:00-06:00 with a more than $+0.2 \mu\text{m}^3 \text{cm}^{-3}$ difference (Fig. 6). This increase
249 in predicted levels was due to an increase in traffic emissions. For the second half of the day, predicted and measured
250 values were in reasonable agreement. Excluding the first two days, which were influenced by the initial conditions, the
251 model overpredicted nighttime to early morning concentrations in several periods (June 10-12, 16-17, 24 and 26) (Fig.
252 S1). Measured concentrations were rarely higher than those predicted, for example on July 2 and 3, when sharp peaks
253 indicated possible nearby sources. The overprediction could indicate that emissions of UFPs in the area were
254 overpredicted.

255 The average diurnal profiles of measured and predicted $PV_{0.1}$ concentrations as well as their corresponding
256 hourly levels for the rest of the 12 sites for the summer period can be found in Figure S1 and Figure S2. PMCAMx-UF
257 reproduced well the average diurnal profile of measured $PV_{0.1}$ in Hyytiala, with an average value of $0.25 \mu\text{m}^3 \text{cm}^{-3}$, while
258 there were overpredictions during the whole day for Vavihill, Waldhof and Aspvreten.

259

260 4.3.2 Winter

261 PMCAMx-UF tended to underpredict the winter $PV_{0.1}$ levels with a NMB equal to -30% for hourly averaged values
262 (Table 2). The NME for hourly predictions was higher than during the summer with a value of 72%. For daily average
263 levels, the NMB was -27% and the NME equal to 64% (Table S2). The model overpredicted $PV_{0.1}$ by 0.03 to $0.09 \mu\text{m}^3$
264 cm^{-3} in the sites of Vavihill, Hyytiala, Aspvreten and Varrio.

265 Mean predicted values in 9 out of 12 sites were within $0.1 \mu\text{m}^3 \text{cm}^{-3}$ of the measured mean (Fig. 7). $PV_{0.1}$ was
266 underpredicted in 7 out of 12 sites. Despite the increased frequency of underprediction, major positive deviations between
267 predictions and observations were found in the Varrio and Hyytiala sites, with high model error also in the Aspvreten,
268 Vavihill, Mace Head and Dresden sites. Mean predicted $PV_{0.1}$ was $0.17 \mu\text{m}^3 \text{cm}^{-3}$ for all sites and mean measured $PV_{0.1}$
269 was $0.24 \mu\text{m}^3 \text{cm}^{-3}$.



270 In Dresden, the ultrafine particle volume concentration was seriously underpredicted, $0.27 \mu\text{m}^3 \text{cm}^{-3}$ to $1.22 \mu\text{m}^3$
271 cm^{-3} respectively. Mean ultrafine particle volume concentration for Helsinki was also underpredicted, with a predicted
272 value of $0.18 \mu\text{m}^3 \text{cm}^{-3}$ and a measured value of $0.35 \mu\text{m}^3 \text{cm}^{-3}$. On the other hand, for the remote Hyytiälä site in Finland,
273 mean predicted total $\text{PV}_{0.1}$ was $0.16 \mu\text{m}^3 \text{cm}^{-3}$, compared to a measured average of $0.07 \mu\text{m}^3 \text{cm}^{-3}$. This suggests that the
274 underpredictions in Helsinki were mostly due to local sources and not to regional underprediction.

275 In Dresden, the measured levels increased by a factor of two early in the morning while the predicted profile
276 remained practically flat (Fig. 8). This suggests strongly the lack of one or more major local sources, probably
277 transportation and residential heating. It could also be partially due to the coarse resolution of the model; local emissions
278 were diluted in the large computational cell of the model covering the area of the city. The corresponding hourly
279 concentrations are shown in Figure S4.

280 For Helsinki, the predicted average diurnal profile was nearly flat (variation less than $0.05 \mu\text{m}^3 \text{cm}^{-3}$) throughout
281 the day, while the measurements peaked at 10:00, remaining near constant during midday and then gradually decreasing
282 (Fig. 8). The hourly concentrations suggested that the model was rarely able to reproduce observed elevated concentration
283 levels during specific one to two-day periods (Fig. S4). The sources of ultrafine particles during these periods need to be
284 further examined. Errors in the meteorological inputs and especially the mixing height were also a possible explanation
285 of these persistent errors.

286 In Hyytiälä, the diurnal average profiles of measured and predicted values were both flat but they differed by
287 approximately $0.1 \mu\text{m}^3 \text{cm}^{-3}$ (Fig. 8). This suggests that the model agreed with observations regarding the relatively low
288 local contributions but it overpredicted the regional background. This could be partially due to the assumed boundary
289 conditions that influenced the Nordic countries more than the rest of Europe due to the choice of modeling domain.
290 Turning our attention to the full period hourly concentrations, substantial deviations became readily apparent (Fig. S4).
291 For the first half of the simulated period, predicted UFP volume concentrations tended to follow measured values, with
292 rapid increases in measured concentrations not generally predicted. These were again possibly indicative of local sources
293 influencing the measurement site. After January 17, the model overpredicted $\text{PV}_{0.1}$. The reasons for this overprediction
294 require future analysis. The average diurnal profiles as well as their corresponding hourly $\text{PV}_{0.1}$ concentrations for the
295 rest of the 12 sites for this winter period can be found in Figure S3 and Figure S4.

296

297 **4.4 Predicted links between $\text{PM}_{0.1}$ and $\text{PM}_{2.5}$**

298 The correlation of predicted $\text{PM}_{2.5}$ with $\text{PM}_{0.1}$ was examined during the summer and winter period. For the summer period,
299 the mass concentration of fine and ultrafine particles had low correlation in Zurich, Bucharest and Helsinki, with
300 comparatively better correlations in Athens, Birmingham and Paris (Fig. 9). In Helsinki, the two values have a coefficient
301 of determination (R^2) of 0.01. Ultrafine particle mass in Helsinki, as well as in Bucharest and Zurich was mostly secondary
302 inorganic and organic during the summer period. In Athens, Paris and Birmingham, the correlation was significantly
303 better, around 0.4 to 0.6. For Athens, the correlation was driven by wildfire episode (Fig. S5). If this period is excluded
304 the correlation decreases significantly.

305 For the winter period, correlations were high across most major cities examined, with the notable exceptions of
306 Bucharest and Birmingham (Fig. S6). The R^2 for Zurich, Birmingham, Bucharest and Helsinki was less than or equal to
307 0.4, but it was higher for Athens (0.71) and Paris (0.65).



308 For most major cities, an increase in the primary component of $PM_{0.1}$, was accompanied with an increase in its
309 correlation with $PM_{2.5}$. The exceptions were again Birmingham and Bucharest. The predicted R^2 value in both cities seems
310 to be influenced by outliers of substantially elevated $PM_{2.5}$ values. Yu et al. (2019) reported an R^2 between predicted $PM_{2.5}$
311 and $PM_{0.1}$ in a year-long study in California, for all domain cells, of 0.63. In that study, $PM_{0.1}$ was mostly comprised of
312 primary matter from combustion processes. This value is comparable to the highest observed in our study, specifically in
313 Athens and Paris.

314

315 5. Conclusions

316 Predicted levels of $PM_{0.1}$ were quite variable in space and time. The average predicted total $PM_{0.1}$ for Europe was $0.6 \mu\text{g}$
317 m^{-3} for the summer and $0.3 \mu\text{g} \text{m}^{-3}$ for the winter period. On average, sulfate (38%), SOA (32%), ammonium (13%) and
318 POA (8%) were the most significant $PM_{0.1}$ components during the summer. Primary and secondary inorganic matter had
319 an increased mass fraction (16% to 23% and 51% to 66%) during the winter period. The secondary organic matter
320 percentage contribution was quite low (6%) during the winter. The high secondary contribution to $PM_{0.1}$ is rather
321 surprising.

322 $PM_{0.1}$ during the winter period correlates better ($R^2=0.18-0.71$) with $PM_{2.5}$ than during the summer period
323 ($R^2=0.01-0.6$). However, for most major cities the correlation is low. Better correlations were observed in cases where
324 primary sources contributed significantly to $PM_{0.1}$.

325 PMCAMx-UF showed little bias (15%) in reproducing the summertime ultrafine volume observations in 12 sites
326 in Europe. During the winter, the model tended to underpredict $PM_{0.1}$ with a NMB of -30% for hourly average values.
327 The model NME for daily average levels was 46% during the summer and 64% during the winter. Using the CTM
328 performance criteria for $PM_{2.5}$, the model performance was considered good for the summer and average for the winter.
329 Missing winter sources need additional investigation.

330 Given that this is the first effort to predict $PM_{0.1}$ in Europe with PMCAMx-UF, the model performance was quite
331 encouraging. Potential model improvements include corrections in emissions especially during the winter, use of higher
332 grid resolution for the major urban areas and revisiting of the boundary conditions over the northern Atlantic. Evaluation
333 of its composition predictions is also needed.

334 The predicted lack of correlation between ultrafine and fine particle mass concentration suggests different
335 sources and processes and that future emission reduction strategies will have different effects on $PM_{0.1}$ and $PM_{2.5}$.

336

337 **Code and Data Availability.** The model code and data used in this study are available from the authors upon request
338 (spyros@chemeng.upatras.gr).

339

340 **Author Contributions.** KM carried out the simulations, the analysis, ES wrote the final manuscript with support from SNP,
341 KM and DP, SNP supervised and coordinated the work.

342

343 **Competing Interests.** The authors declare no competing financial interest.

344

345 **Acknowledgements.** This work was supported by «Atmospheric nanoparticles, air quality and human health»,
346 NANOSOMs (11504) and the EU H2020 RI-URBANS (grant 101036245) project.



347

348 **References**

- 349 del Águila, A., Sorribas, M., Lyamani, H., Titos, G., Olmo, F. J., Arruda-Moreira, G., Yela, M., and Alados-Arboledas,
350 L.: Sources and physicochemical characteristics of submicron aerosols during three intensive campaigns in
351 Granada (Spain), *Atmos. Res.*, 213, 398–410, <https://doi.org/10.1016/j.atmosres.2018.06.004>, 2018.
- 352 Argyropoulou, G., Patoulias, D., and Pandis, S. N.: Exploring the potential for continuous measurement of ultrafine
353 particle mass concentration ($PM_{0.1}$) based on measurements of particle number concentration above 50 nm (N_{50}),
354 *Aerosol Science and Technology*, 57, 1117–1127, <https://doi.org/10.1080/02786826.2023.2249075>, 2023.
- 355 Argyropoulou, G. A., Kaltsonoudis, C., Patoulias, D., and Pandis, S. N.: Novel method for the continuous mass
356 concentration measurement of ultrafine particles ($PM_{0.1}$) with a water-based condensation particle counter
357 (CPC), *Aerosol Science and Technology*, 1–12, <https://doi.org/10.1080/02786826.2024.2368196>, 2024.
- 358 Baranizadeh, E., Murphy, N. B., Julin, J., Falahat, S., Reddington, L. C., Arola, A., Ahlm, L., Mikkonen, S., Fountoukis,
359 C., Patoulias, D., Minikin, A., Hamburger, T., Laaksonen, A., Pandis, N. S., Vehkamäki, H., Lehtinen, E. J. K.,
360 and Riipinen, I.: Implementation of state-of-the-art ternary new-particle formation scheme to the regional
361 chemical transport model PMCAMx-UF in Europe, *Geosci. Model. Dev.*, 9, 2741–2754,
362 <https://doi.org/10.5194/GMD-9-2741-2016>, 2016.
- 363 Bernardoni, V., Elser, M., Valli, G., Valentini, S., Bigi, A., Fermo, P., Piazzalunga, A., and Vecchi, R.: Size-segregated
364 aerosol in a hot-spot pollution urban area: Chemical composition and three-way source apportionment, *Environ.*
365 *Pollut.*, 231, 601–611, <https://doi.org/10.1016/j.envpol.2017.08.040>, 2017.
- 366 Colella, P. and Woodward, P. R.: The Piecewise Parabolic Method (PPM) for gas-dynamical simulations, *J. Comput.*
367 *Phys.*, 54, 174–201, [https://doi.org/10.1016/0021-9991\(84\)90143-8](https://doi.org/10.1016/0021-9991(84)90143-8), 1984.
- 368 Delfino, R. J., Sioutas, C., and Malik, S.: Potential role of ultrafine particles in associations between airborne particle
369 mass and cardiovascular health, *Environ Health Perspect*, 113, 934, <https://doi.org/10.1289/EHP.7938>, 2005.
- 370 ENVIRON: Environ: User's guide to the comprehensive air quality model with extensions (CAMx), version 4.02, Novato,
371 CA, 2003.
- 372 Environmental Protection Agency, United States: Integrated science assessment (ISA) for particulate matter, Washington,
373 DC: US Environmental Protection Agency, 2019.
- 374 Fahey, K. M. and Pandis, S. N.: Optimizing model performance: variable size resolution in cloud chemistry modeling,
375 *Atmos. Environ.*, 35, 4471–4478, [https://doi.org/10.1016/S1352-2310\(01\)00224-2](https://doi.org/10.1016/S1352-2310(01)00224-2), 2001.
- 376 Gaydos, T. M., Pinder, R., Koo, B., Fahey, K. M., Yarwood, G., and Pandis, S. N.: Development and application of a
377 three-dimensional aerosol chemical transport model, *PMCAMx*, *Atmos. Environ.*, 41, 2594–2611,
378 <https://doi.org/10.1016/j.atmosenv.2006.11.034>, 2007.
- 379 Guenther, A., Karl, T., Harley, P., Wiedinmyer, C., Palmer, P. I., and Geron, C.: Estimates of global terrestrial isoprene
380 emissions using MEGAN (Model of Emissions of Gases and Aerosols from Nature), *Atmos. Chem. Phys.*, 6,
381 3181–3210, <https://doi.org/10.5194/ACP-6-3181-2006>, 2006.
- 382 HEI Report: Review panel on ultrafine particles, Understanding the health effects of ambient ultrafine particles HEI
383 Perspectives 3Health Effects Institute, Boston, MA, 122, 2013.



- 384 Hu, J., Zhang, H., Chen, S., Ying, Q., Wiedinmyer, C., Vandenberghe, F., and Kleeman, M. J.: Identifying PM_{2.5} and
385 PM_{0.1} sources for epidemiological studies in California, *Environ. Sci. Technol.*, 48, 4980–4990, [https://doi.org/](https://doi.org/10.1021/ES404810Z)
386 10.1021/ES404810Z, 2014a.
- 387 Hu, J., Zhang, H., Chen, S. H., Wiedinmyer, C., Vandenberghe, F., Ying, Q., and Kleeman, M. J.: Predicting primary
388 PM_{2.5} and PM_{0.1} trace composition for epidemiological studies in California, *Environ. Sci. Technol.*, 48, 4971–
389 4979, 2014b.
- 390 Hu, J., Jathar, S., Zhang, H., Ying, Q., Chen, S. H., Cappa, C. D., and Kleeman, M. J.: Long-term particulate matter
391 modeling for health effect studies in California - Part 2: Concentrations and sources of ultrafine organic aerosols,
392 *Atmos. Chem. Phys.*, 17, 5379–5391, <https://doi.org/10.5194/ACP-17-5379-2017>, 2017.
- 393 Hughes, L. S., Cass, G. R., Gone, J., Ames, M., and Olmez, I.: Physical and chemical characterization of atmospheric
394 ultrafine particles in the Los Angeles area, *Environ. Sci. Technol.*, 32, 1153–1161, 1998.
- 395 Jung, J. G., Fountoukis, C., Adams, P. J., and Pandis, S. N.: Simulation of in situ ultrafine particle formation in the eastern
396 United States using PMCAMx-UF, *J. Geophys. Res.*, 115, <https://doi.org/10.1029/2009JD012313>, 2010.
- 397 Kleeman, M. J., Riddle, S. G., Robert, M. A., Jakober, C. A., Fine, P. M., Hays, M. D., Schauer, J. J., and Hannigan, M.
398 P.: Source apportionment of fine (PM_{1.8}) and ultrafine (PM_{0.1}) airborne particulate matter during a severe winter
399 pollution episode, *Environ. Sci. Technol.*, 43, 272–279, 2009.
- 400 Kulmala, M., Asmi, A., Lappalainen, H. K., Baltensperger, U., Brenguier, J. L., Facchini, M. C., Hansson, H. C., Hov,
401 O’Dowd, C. D., Pöschl, U., Wiedensohler, A., Boers, R., Boucher, O., De Leeuw, G., Denier Van Der Gon, H.
402 A. C., Feichter, J., Krejci, R., Laj, P., Lihavainen, H., Lohmann, U., McFiggans, G., Mentel, T., Pilinis, C.,
403 Riipinen, I., Schulz, M., Stohl, A., Swietlicki, E., Vignati, E., Alves, C., Amann, M., Ammann, M., Arabas, S.,
404 Artaxo, P., Baars, H., Beddows, D. C. S., Bergström, R., Beukes, J. P., Bilde, M., Burkhardt, J. F., Canonaco, F.,
405 Clegg, S. L., Coe, H., Crumeyrolle, S., D’Anna, B., Decesari, S., Gilardoni, S., Fischer, M., Fjaeraa, A. M.,
406 Fountoukis, C., George, C., Gomes, L., Halloran, P., Hamburger, T., Harrison, R. M., Herrmann, H., Hoffmann,
407 T., Hoese, C., Hu, M., Hyvärinen, A., Hörrak, U., Iinuma, Y., Iversen, T., Josipovic, M., Kanakidou, M.,
408 Kiendler-Scharr, A., Kirkevåg, A., Kiss, G., Klimont, Z., Kolmonen, P., Komppula, M., Kristjánsson, J. E.,
409 Laakso, L., Laaksonen, A., Labonnote, L., Lanz, V. A., Lehtinen, K. E. J., Rizzo, L. V., Makkonen, R.,
410 Manninen, H. E., McMeeking, G., Merikanto, J., Minikin, A., Mirme, S., Morgan, W. T., Nemitz, E., O’Donnell,
411 D., Panwar, T. S., Pawlowska, H., Petzold, A., Pienaar, J. J., Pio, C., Plass-Duelmer, C., Prévôt, A. S. H., Pryor,
412 S., Reddington, C. L., Roberts, G., Rosenfeld, D., Schwarz, J., Seland, O., et al.: General overview: European
413 Integrated project on Aerosol Cloud Climate and Air Quality interactions (EUCAARI)-integrating aerosol
414 research from nano to global scales, *Atmos. Chem. Phys.*, 11, 13061–130143, [https://doi.org/10.5194/ACP-11-](https://doi.org/10.5194/ACP-11-13061-2011)
415 13061-2011, 2011.
- 416 Kuwayama, T., Ruehl, C. R., and Kleeman, M. J.: Daily trends and source apportionment of ultrafine particulate mass
417 (PM_{0.1}) over an annual cycle in a typical California city, *Environ. Sci. Technol.*, 47, 13957–13966, 2013.
- 418 Kwon, H. S., Ryu, M. H., and Carlsen, C.: Ultrafine particles: unique physicochemical properties relevant to health and
419 disease, *Experimental & Molecular Medicine* 2020 52:3, 52, 318–328, [https://doi.org/10.1038/s12276-020-](https://doi.org/10.1038/s12276-020-0405-1)
420 0405-1, 2020.
- 421 Merikanto, J., Spracklen, D. V., Mann, G. W., Pickering, S. J., and Carslaw, K. S.: Impact of nucleation on global CCN,
422 *Atmos. Chem. Phys.*, 9, 8601–8616, <https://doi.org/10.5194/ACP-9-8601-2009>, 2009.



- 423 Odman, M. and Ingram, C.: Multiscale Air Quality Simulation Platform (MAQSIP): Source code documentation and
424 validation, 1996.
- 425 O’Dowd, C. D., Langmann, B., Varghese, S., Scannell, C., Ceburnis, D., and Facchini, M. C.: A combined organic-
426 inorganic sea-spray source function, *Geophys. Res. Lett.*, 35, <https://doi.org/10.1029/2007GL030331>, 2008.
- 427 Ohlwein, S., Kappeler, R., Kutlar Joss, M., Künzli, N., and Hoffmann, B.: Health effects of ultrafine particles: a systematic
428 literature review update of epidemiological evidence, *Int. J. Public Health*, 64, 547–559,
429 <https://doi.org/10.1007/S00038-019-01202-7>, 2019.
- 430 Patoulias, D.: Simulation of the formation and growth of atmospheric nanoparticles. Diss. University of Patras, 2017
- 431 Patoulias, D. and Pandis, S. N.: Simulation of the effects of low-volatility organic compounds on aerosol number
432 concentrations in Europe, *Atmos. Chem. Phys.*, 22, 1689–1706, <https://doi.org/10.5194/ACP-22-1689-2022>,
433 2022.
- 434 Patoulias, D., Fountoukis, C., Riipinen, I., and Pandis, S. N.: The role of organic condensation on ultrafine particle growth
435 during nucleation events, *Atmos. Chem. Phys.*, 15, 6337–6350, <https://doi.org/10.5194/ACP-15-6337-2015>,
436 2015.
- 437 Patoulias, D., Fountoukis, C., Riipinen, I., Asmi, A., Kulmala, M., and Pandis, S. N.: Simulation of the size-composition
438 distribution of atmospheric nanoparticles over Europe, *Atmos. Chem. Phys.*, 18, 13639–13654,
439 <https://doi.org/10.5194/ACP-18-13639-2018>, 2018.
- 440 Phairuang, W., Inerb, M., Hata, M., and Furuuchi, M.: Characteristics of trace elements bound to ambient nanoparticles
441 (PM_{0.1}) and a health risk assessment in southern Thailand, *J. Hazard. Mater.*, 425, 127986, 2022.
- 442 Putaud, J. P., Van Dingenen, R., Alastuey, A., Bauer, H., Birmili, W., Cyrys, J., Flentje, H., Fuzzi, S., Gehrig, R., Hansson,
443 H. C., Harrison, R. M., Herrmann, H., Hitznerberger, R., Hüglin, C., Jones, A. M., Kasper-Giebl, A., Kiss, G.,
444 Koussa, A., Kuhlbusch, T. A. J., Löschau, G., Maenhaut, W., Molnar, A., Moreno, T., Pekkanen, J., Perrino, C.,
445 Pitz, M., Puxbaum, H., Querol, X., Rodriguez, S., Salma, I., Schwarz, J., Smolik, J., Schneider, J., Spindler, G.,
446 ten Brink, H., Tursic, J., Viana, M., Wiedensohler, A., and Raes, F.: A European aerosol phenomenology – 3:
447 Physical and chemical characteristics of particulate matter from 60 rural, urban, and kerbside sites across Europe,
448 *Atmos. Environ.*, 44, 1308–1320, <https://doi.org/10.1016/J.ATMOSENV.2009.12.011>, 2010.
- 449 Schraufnagel, D. E.: The health effects of ultrafine particles, *Exp. Mol. Med.*, 52, 311–317,
450 <https://doi.org/10.1038/S12276-020-0403-3>, 2020.
- 451 Seinfeld, J. H. and Pandis, S. N.: Atmospheric Chemistry and Physics of Air Pollution- From Air Pollution to Climate
452 Change, 2nd Edition, John Wiley & Sons, 2006.
- 453 Sioutas, C., Delfino, R. J., and Singh, M.: Exposure assessment for atmospheric ultrafine particles (UFPs) and
454 implications in epidemiologic research, *Environ Health Perspect.*, 113, 947–955,
455 <https://doi.org/10.1289/EHP.7939>, 2005.
- 456 Skamarock, W. C., Klemp, J. B., Dudhi, J., Gill, D. O., Barker, D. M., Duda, M. G., Huang, X.-Y., Wang, W., and Powers,
457 J. G.: A Description of the Advanced Research WRF Version 2, Technical Report, 113,
458 <https://doi.org/10.5065/D6DZ069T>, 2005.
- 459 Slinn, S. A. and Slinn, W. G. N.: Predictions for particle deposition on natural waters, *Atmos. Environ.*, 14, 1013–1016,
460 [https://doi.org/10.1016/0004-6981\(80\)90032-3](https://doi.org/10.1016/0004-6981(80)90032-3), 1980.



- 461 Sofiev, M., Lanne, M., Vankevich, R., Prank, M., Karppinen, A., and Kukkonen, J.: Impact of wild-land fires on European
462 air quality in 2006–2008, *WIT Transactions on Ecology and the Environment*, 119, 353–361,
463 <https://doi.org/10.2495/FIVA080351>, 2008a.
- 464 Sofiev, M., Vankevich, R., Lanne, M., Koskinen, J., and Kukkonen, J.: On integration of a fire assimilation system and a
465 chemical transport model for near-real time monitoring of the impact of wild-land fires on atmospheric
466 composition and air quality, *WIT Transactions on Ecology and the Environment*, 119, 343–351,
467 <https://doi.org/10.2495/FIVA080341>, 2008b.
- 468 Venecek, M. A., Yu, X., and Kleeman, M. J.: Predicted ultrafine particulate matter source contribution across the
469 continental United States during summertime air pollution events, *Atmos. Chem. Phys.*, 19, 9399–9412,
470 <https://doi.org/10.5194/ACP-19-9399-2019>, 2019.
- 471 Wang, M. and Penner, J. E.: Aerosol indirect forcing in a global model with particle nucleation, *Atmos. Chem. Phys.*, 9,
472 239–260, <https://doi.org/10.5194/acp-9-239-2009>, 2009.
- 473 Weichenthal, S., Olaniyan, T., Christidis, T., Lavigne, E., Hatzopoulou, M., Van Ryswyk, K., Tjepkema, M., and Burnett,
474 R.: Within-city spatial variations in ambient ultrafine particle concentrations and incident brain tumors in adults,
475 *Epidemiology*, 31, 177–183, 2020.
- 476 Wesely, M. L.: Parameterization of surface resistances to gaseous dry deposition in regional-scale numerical models,
477 *Atmos. Environ.*, 23, 1293–1304, [https://doi.org/10.1016/0004-6981\(89\)90153-4](https://doi.org/10.1016/0004-6981(89)90153-4), 1989.
- 478 Xue, J., Li, Y., Peppers, J., Wan, C., Kado, N. Y., Green, P. G., Young, T. M., and Kleeman, M. J.: Ultrafine particle
479 emissions from natural gas, biogas, and biomethane combustion, *Environ Sci Technol*, 52, 13619–13628, 2018.
- 480 Xue, J., Xue, W., Sowlat, M. H., Sioutas, C., Lolincio, A., Hasson, A., and Kleeman, M. J.: Seasonal and annual source
481 appointment of carbonaceous ultrafine particulate matter (PM_{0.1}) in polluted California cities, *Environ. Sci.
482 Technol.*, 53, 39–49, 2019.
- 483 Xue, W. and Kleeman, M. J.: Comparison of size-resolved PM elements measured using aluminum foil and Teflon
484 impaction substrates: Implications for ultrafine particle source apportionment and future sampling networks in
485 California, *Sci. Total Environ.*, 838, 156523, <https://doi.org/10.1016/j.scitotenv.2022.156523>, 2022.
- 486 Xue, W., Xue, J., Shirmohammadi, F., Sioutas, C., Lolincio, A., Hasson, A., and Kleeman, M. J.: Day-of-week patterns
487 for ultrafine particulate matter components at four sites in California, *Atmos Environ*, 222, 117088,
488 <https://doi.org/10.1016/j.atmosenv.2019.117088>, 2020a.
- 489 Xue, W., Xue, J., Mousavi, A., Sioutas, C., and Kleeman, M. J.: Positive matrix factorization of ultrafine particle mass
490 (PM_{0.1}) at three sites in California, *Sci. Total Environ.*, 715, 136902,
491 <https://doi.org/10.1016/j.scitotenv.2020.136902>, 2020b.
- 492 Yu, F. and Luo, G.: Simulation of particle size distribution with a global aerosol model: Contribution of nucleation to
493 aerosol and CCN number concentrations, *Atmos. Chem. Phys.*, 9, 7691–7710, <https://doi.org/10.5194/ACP-9-7691-2009>, 2009.
- 495 Yu, X., Venecek, M., Kumar, A., Hu, J., Tanrikulu, S., Soon, S. T., Tran, C., Fairley, D., and Kleeman, M. J.: Regional
496 sources of airborne ultrafine particle number and mass concentrations in California, *Atmos. Chem. Phys.*, 19,
497 14677–14702, <https://doi.org/10.5194/acp-19-14677-2019>, 2019.



498 Zhu, Y., Hinds, W. C., Kim, S., and Sioutas, C.: Concentration and size distribution of ultrafine particles near a major
499 highway, *J. Air. Waste. Manage. Assoc.*, 52, 1032–1042, <https://doi.org/10.1080/10473289.2002.10470842>,
500 2002.
501
502



503
504

Table 1. PMCAMx-UF hourly evaluation metrics of $PV_{0.1}$ during the period of 5 June - 8 July 2012 for the 12 measurement sites.

Station	Mean Predicted ($\mu\text{m}^3 \text{ cm}^{-3}$)	Mean Observed ($\mu\text{m}^3 \text{ cm}^{-3}$)	NMB (%)	NME (%)
Dresden	0.42	0.59	-29	45
Kosetice	0.37	0.24	54	82
Hohenpeissenberg	0.22	0.27	-19	49
Mace Head	0.05	0.06	-5	81
Finokalia	0.39	0.36	6	47
Vavihill	0.47	0.28	66	82
Helsinki	0.44	0.48	-9	44
Melpitz	0.41	0.33	21	61
Hyytiala	0.22	0.23	-3	61
Waldhof	0.50	0.31	63	81
Aspvreten	0.48	0.23	109	125
Varrio	0.10	0.10	-8	68

505
506
507
508
509
510
511
512
513
514
515
516
517
518
519
520

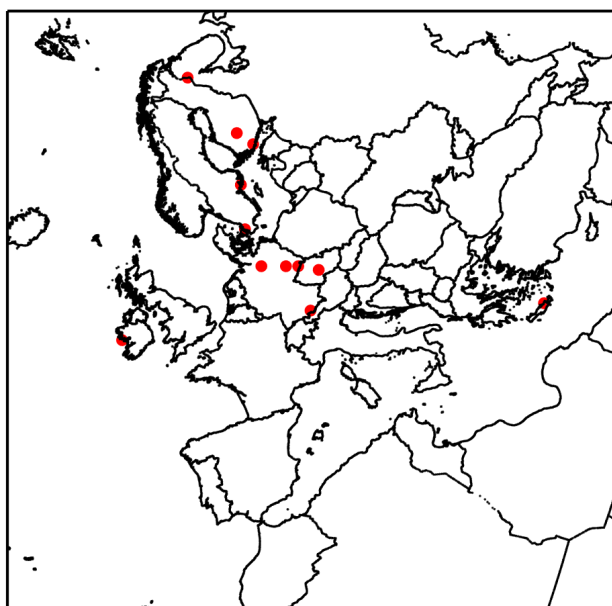


521
522

Table 2. PMCAMx-UF hourly evaluation metrics of $PV_{0.1}$ during the period of 1-30 January 2009 for the 12 measurement sites.

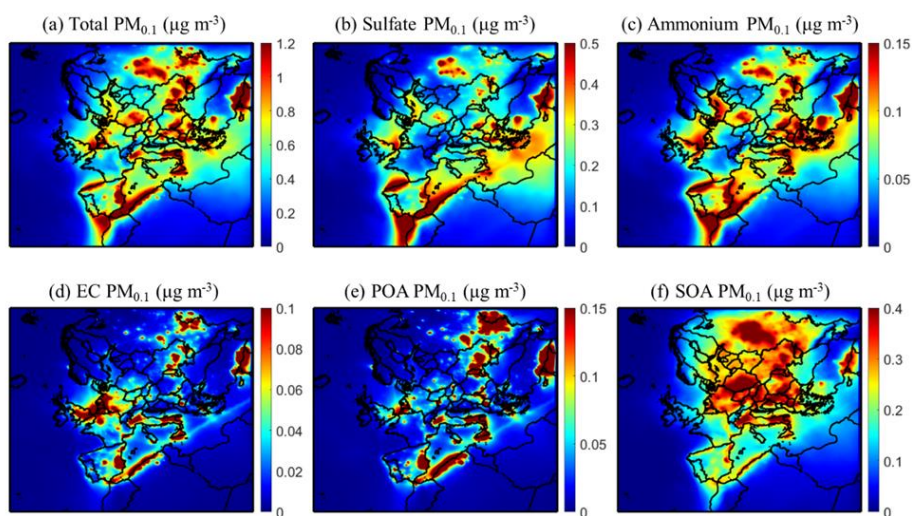
Station	Mean Predicted ($\mu\text{m}^3 \text{cm}^{-3}$)	Mean Observed ($\mu\text{m}^3 \text{cm}^{-3}$)	NMB (%)	NME (%)
Dresden	0.27	1.22	-78	78
Kosetice	0.24	0.46	-47	56
Hohenpeissenberg	0.16	0.18	-16	51
Mace Head	0.02	0.11	-78	82
Finokalia	0.07	0.14	-48	65
Vavihill	0.25	0.20	27	83
Helsinki	0.18	0.35	-50	66
Melpitz	0.27	0.28	-6	52
Hyytiala	0.16	0.07	130	187
Waldhof	0.27	0.27	3	53
Aspvreten	0.11	0.08	33.5	114
Varrio	0.09	0.02	399	436

523



524
525
526
527
528
529
530
531
532
533
534
535
536
537
538
539
540
541
542
543
544
545

Figure 1. Map of the European modelling domain indicating (red dots) the 12 measurement sites with available particle number distribution measurements for both simulation periods.



546

547 **Figure 2.** Average predicted ground level $PM_{0.1}$ mass concentrations ($\mu g m^{-3}$) of (a) total $PM_{0.1}$, (b) $PM_{0.1}$ sulfate, (c)
548 $PM_{0.1}$ ammonium, (d) $PM_{0.1}$ elemental carbon, (e) $PM_{0.1}$ primary organic aerosol and (f) $PM_{0.1}$ secondary organic aerosol
549 during 5 June - 8 July 2012.
550



551
552
553
554
555
556
557
558
559
560
561
562
563
564
565
566
567
568
569
570
571
572
573
574
575
576
577
578
579
580
581
582
583
584
585
586
587
588
589
590
591
592

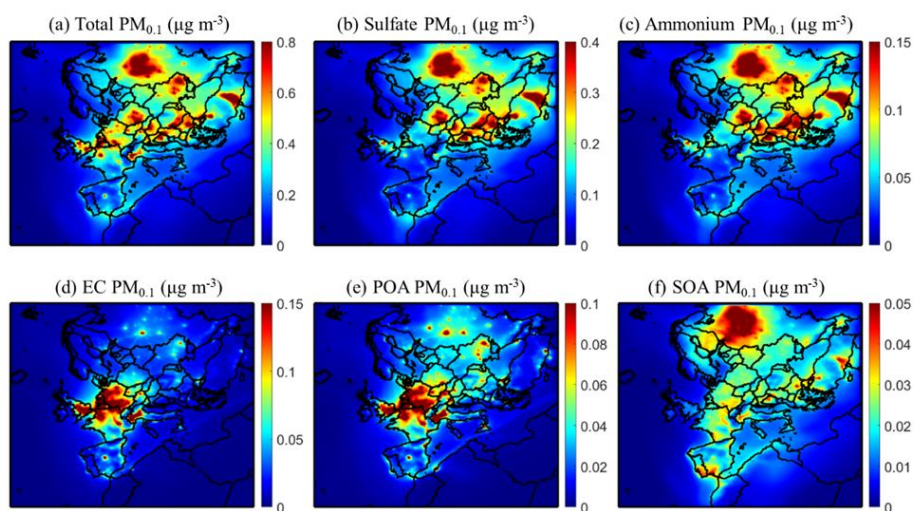
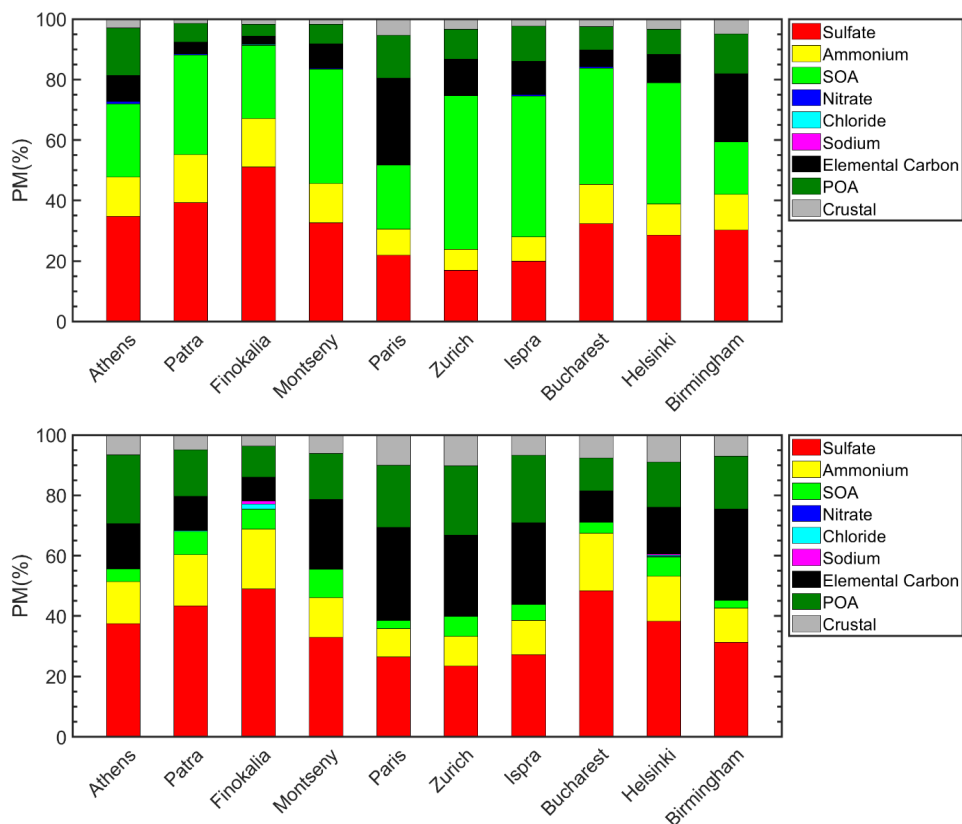


Figure 3. Average predicted ground level $PM_{0.1}$ mass concentrations ($\mu\text{g m}^{-3}$) of (a) total $PM_{0.1}$, (b) $PM_{0.1}$ sulfate, (c) $PM_{0.1}$ ammonium, (d) $PM_{0.1}$ elemental carbon, (e) $PM_{0.1}$ primary organic aerosol and (f) $PM_{0.1}$ secondary organic aerosol during 1 - 30 January 2009.



593

594 **Figure 4.** Predicted chemical composition of ultrafine particles in the areas studied during the (a) summer and (b) winter
595 period. POA (dark green) and SOA (green) stand for primary and secondary organic aerosol.

596



597
598
599
600
601
602
603
604
605
606
607
608
609
610
611
612
613
614
615
616
617
618
619
620
621
622
623
624
625
626
627
628
629
630
631
632
633

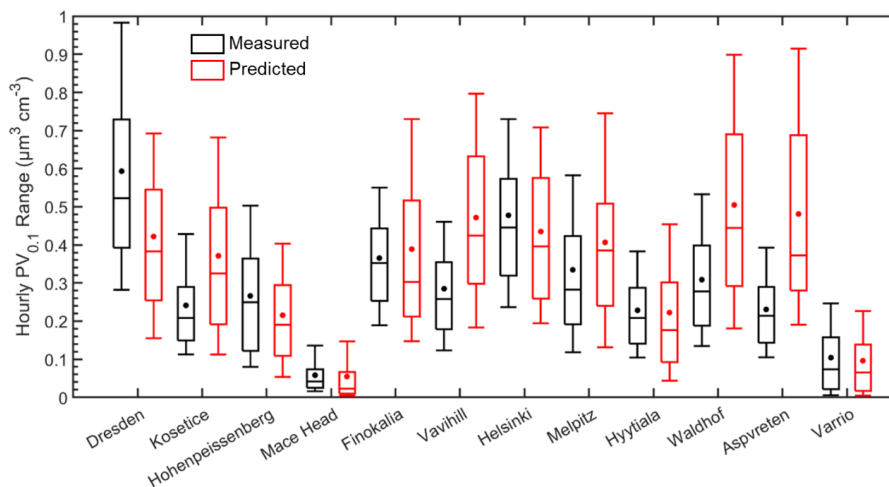


Figure 5. Distributions of predicted (red) and measured (black) hourly ground-level UFP volume (in $\mu\text{m}^3 \text{cm}^{-3}$) during 5 June - 8 July 2012, in the 12 sites examined. Stars and lines inside each box designate the mean and the median value of the PV_{0.1} distribution. Box top and bottom lines indicate the upper (75%) and lower (25%) quartiles. The upper and lower extended lines (whiskers) are for the 90th and the 10th UFP volume distribution percentiles.



634
635
636
637
638
639
640
641
642
643
644
645
646
647
648
649
650
651
652
653
654
655
656
657
658
659
660
661
662
663
664
665
666
667

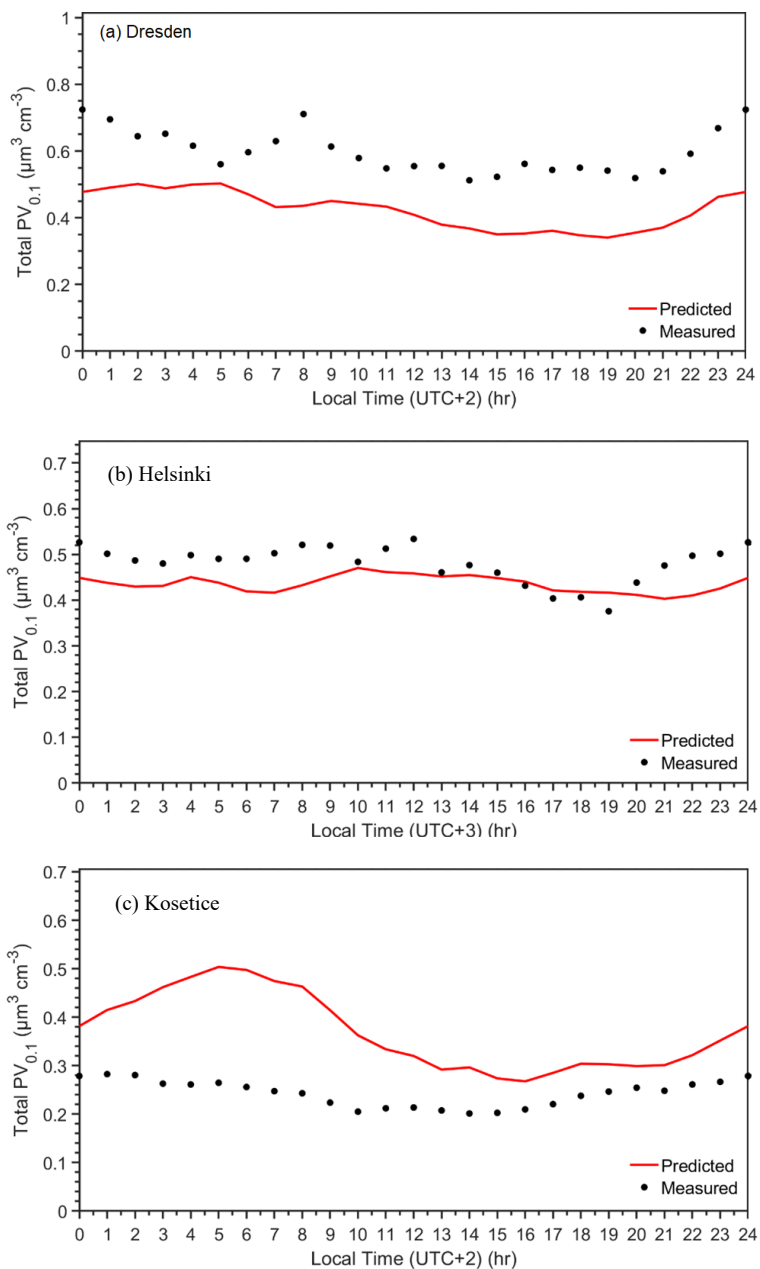
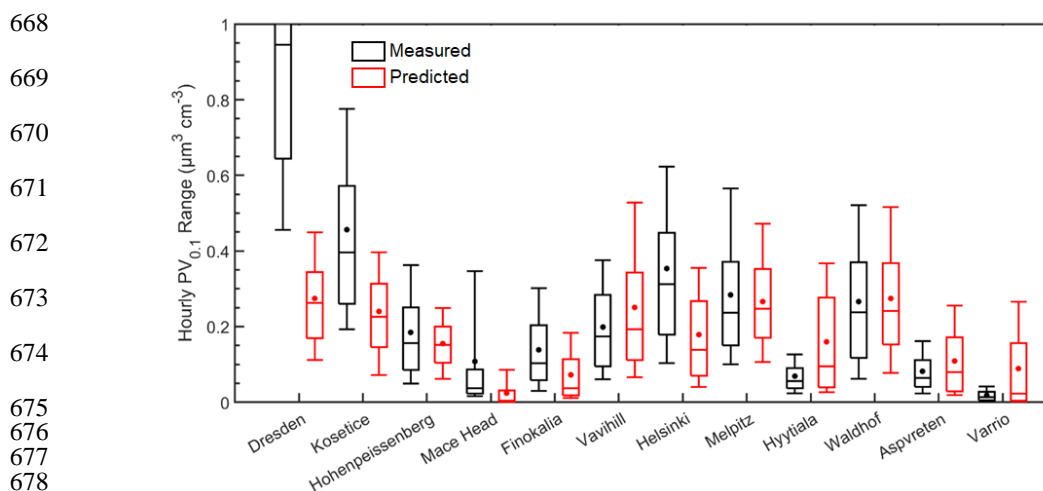


Figure 6. Average diurnal profiles of predicted and measured total volume concentrations ($\mu\text{m}^3 \text{cm}^{-3}$) in (a) Dresden, (b) Helsinki and (c) Kosetice for the period of 5 June - 8 July 2012.



668
669
670
671
672
673
674
675
676
677
678
679
680
681
682
683
684
685
686
687
688
689
690
691
692
693
694
695
696
697
698
699
700
701

Figure 7. Distributions of predicted (red) and measured (black) ground-level UFP volume during 1-30 January 2009, in the 12 sites examined. Stars and lines inside each box designate the mean and the median value of the $PV_{0.1}$ distribution. Box top and bottom lines indicate the upper (75%) and lower (25%) quartiles. The upper and lower extended lines (whiskers) are for the 90th and the 10th UFP volume distribution percentiles.



702

703

704

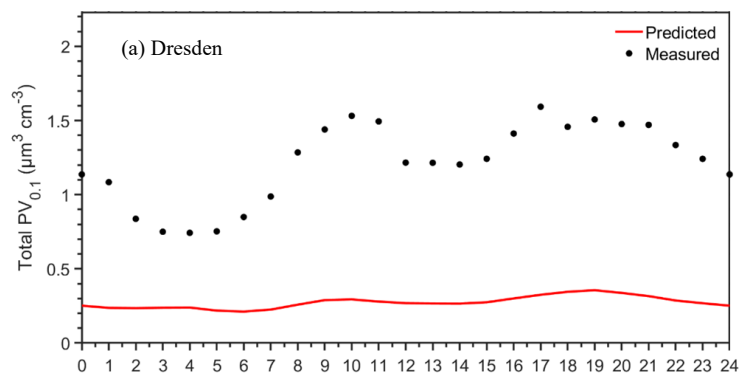
705

706

707

708

709



710

711

712

713

714

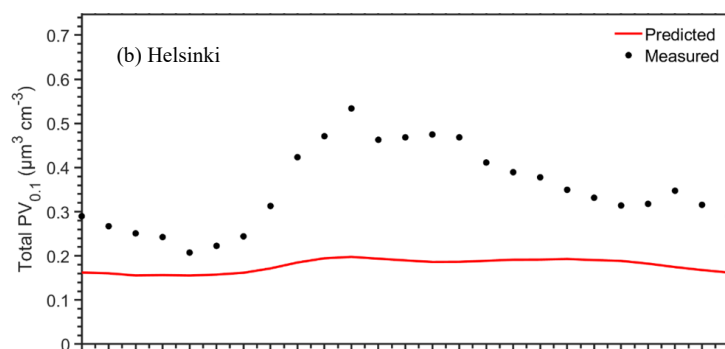
715

716

717

718

719



720

721

722

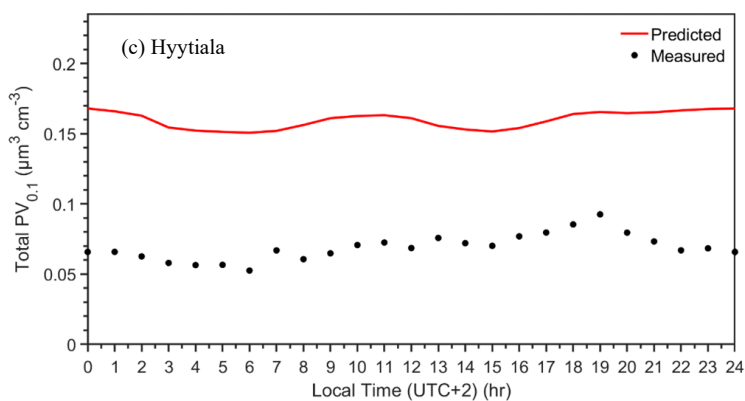
723

724

725

726

727



728

729

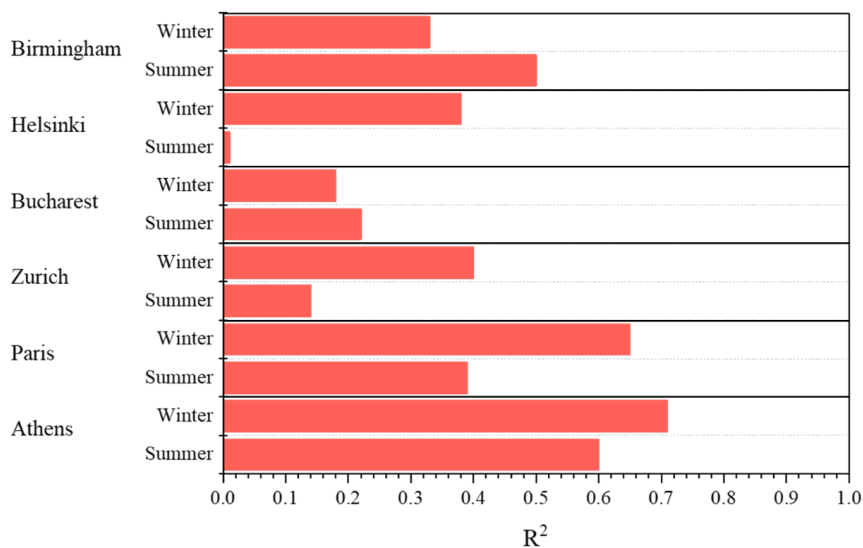
730

731

732 **Figure 8.** Average diurnal profiles of predicted and measured total volume concentrations ($\mu\text{m}^3 \text{cm}^{-3}$) in (a) Dresden, (b)

733 Helsinki and (c) Hyytiälä for the period of 1-30 January 2009.

734



735
736
737
738
739

Figure 9. R² values correspond to the square of the samples Pearson's correlation coefficient R for Athens, Paris, Zurich, Bucharest, Helsinki and Birmingham during the summer and winter periods.